Available online at www.sciencedirect.com
ScienceDirect
International Journal of Impact Engineering 34 (2007) 448–463
INTERNATIONAL JOURNAL OF IMPACT ENGINEERING
www.elsevier.com/locate/ijimpeng

Instability strain and shear band spacing in simple tensile/compressive deformations of thermoviscoplastic materials

R.C. Batra*, Z.G. Wei

Department of Engineering Science and Mechanics, MC 0219, Virginia Polytechnic Institute and State University, Blacksburg, VA 24061, USA

Received 14 April 2005; accepted 10 November 2005
Available online 24 January 2006

Abstract

We analyze the stability of homogeneous simple tensile/compressive deformations of an isotropic heat-conducting thermoviscoplastic bar by studying the growth of infinitesimal perturbations superimposed upon a homogeneous deformation. The smallest axial strain at which the superimposed perturbation has a positive initial growth rate is called the instability strain. Two criteria are used to determine the shear band spacing; (i) the wave number, ξ_m, of the perturbation that has the maximum initial growth rate gives the spacing, $L_s = 2\pi/\xi_m$, between adjacent shear bands, and (ii) $L_s = \inf_{t_0 \geqslant 0} 2\pi/\xi_m(t_0)$ where t_0 is the time when the homogeneous solution is perturbed. It is found that the geometric softening/hardening significantly affects the instability strain and the value of L_s. The effect of varying the thermal conductivity, the strain-rate hardening exponent and the average axial strain rate on L_s has been delineated. It is found that $L_s \propto (\text{nominal axial strain rate})^{-0.757}$. However, for $L_s \propto (\text{thermal conductivity})^{\bar{\chi}}$, the value of $\bar{\chi}$ strongly depends upon the strain rate hardening exponent m. No scaling law is found between L_s and the Taylor–Quinney parameter. For $L_s \propto (\text{specific heat})^{\chi}$, the value of χ depends upon the strain-rate hardening exponent m and increases monotonically with an increase in the value of m.

Keywords: Shear band spacing; Thermoviscoplasticity; Instability criterion; Perturbation method; Scaling laws

1. Introduction

The simple tension test on a metallic bar is widely used for ascertaining mechanical properties of a material. If the load is gradually increased from zero, the bar first deforms elastically, then yields and deforms plastically. At a certain point during the plastic deformations a maximum occurs in the load and the structure becomes unstable. A further increase in the load necks the specimen and it quickly fractures. Considerè [1] proposed that the bar becomes unstable at the maximum in the applied load, and successfully described the competition between strain hardening and the geometric softening caused by the reduction in the cross-section. Considerè's criterion gives a reasonably good estimate of the critical strain for the onset of necking in a bar deformed quasi-statically. Hart [2] proposed an instability criterion based on the growth of an

*Corresponding author. Tel.: +1 540 231 6051; fax: +1 540 231 4574.
E-mail addresses: rbatra@vt.edu (R.C. Batra), zwei@vt.edu (Z.G. Wei).

0734-743X/$ - see front matter © 2005 Elsevier Ltd. All rights reserved.
doi:10.1016/j.ijimpeng.2005.11.004

inhomogeneity in a bar and considered the influence of strain-rate sensitivity of the flow stress. Hart's approach has been adopted by Jonas and Baudelet [3], who studied the effect of crack and cavity generation on instability of a tensile bar. Kocks et al. [4] re-examined the development of nonuniformities in tensile deformations and found that a material may be stable even after Hart's criterion is met. Ferron [5] studied the effect of heat generation due to plastic deformations on the instability of a material. Fressengeas and Molinari [6] used a perturbation method to analyze the instability of plastic flow in a thermoviscoplastic material.

At high strain rates, instability and necking are more complex phenomena than in static case due to inertia, thermal softening, heat conduction and damage evolution, and material fragmentation is frequently encountered. Shockey and Erlich [7], and Shockey [8] described an exploding cylinder technique and presented several observations of metallurgical effects in a steel. This technique eliminates the influence of the loading geometry, and shear bands are produced in the absence of externally induced stress concentrations. Hence, nucleation sites are selected by the material and features associated with the load application rather than by artificial defects introduced in the structure. Furthermore, numerous shear bands occur allowing statistical descriptions of their numbers and sizes. The expansion of the exploding cylinders was stopped before extensive fragmentation could occur, thereby allowing shear bands to be observed in various stages of development and simplifying the recovery procedure for post-test examination. The strain and the strain rate in the specimen can be varied by changing the explosive mixture and the cylinder thickness. Many well-developed shear bands were observed in AISI4340 steel, numerous incipient shear bands in a medium carbon RC24 steel, and none in fine grained RC27 and RC55 tool steels that deformed homogeneously till brittle fracture. Shear bands nucleated at discrete sites on the inner surface of the cylinder and propagated radially outwards along 45° planes achieving a semicircular planar geometry. Nesterenko et al. [9] experimentally investigated the shear band spacing (SBS) in an explosively loaded hollow cylinder with the crack formation impeded by an imposed hydrostatic pressure. If the length of the cylinder is very large as compared to its inner diameter, the explosive charge is uniformly distributed along its length and is ignited instantaneously then a plane strain state of deformation can be assumed to prevail in the cylinder. Xue et al. [10] found that the average strain in shear bands formed in commercially pure titanium equals 0.55 and the average SBS is 0.53 mm; they have also presented a two-dimensional analysis of this problem.

Grady and Kipp [11], and Grady [12] analyzed simple shearing deformations of a thermally softening material and derived an expression for the SBS by accounting for momentum diffusion due to unloading within bands. Bai et al. [13] have deduced an approximate relationship between the shear band thickness and the SBS. They studied deformation patterns using dimensional analysis and found that two diffusion processes, namely heat conduction and momentum transfer, are involved. Within the same time scale, the length scale of heat diffusion is usually much less than that of the momentum transport in metals. The shear band thickness is controlled by heat diffusion and the SBS by momentum diffusion. This difference in diffusion rates may govern the pattern of adiabatic shear bands.

Bai [14] considered simple shearing deformations of a thermoviscoplastic body, perturbed the homogeneous solution of the governing equations, derived equations linear in the amplitude of the perturbation and studied the stability of the homogeneous solution. He defined a characteristic length scale associated with the wavelength of the perturbation corresponding to its maximum initial growth rate. Wright and Ockendon [15] postulated that perturbations growing simultaneously at different sites would never merge, and thus result in multiple shear bands. Hence, the wavelength of the mode with the maximum initial growth rate corresponds to the minimum spacing between shear bands. Molinari [16] generalized Wright and Ockendon's work to strain hardening materials, and by using an asymptotic expansion technique quantified the effect of the strain hardening exponent on the minimum SBS, L_s, defined as $L_s = \inf_{t_0 \geqslant 0}(2\pi/\xi_m(t_0))$. Here, ξ_m is the wave number of the perturbation introduced at time t_0 that has the maximum initial growth rate at t_0. He delineated the error in the minimum SBS caused by the assumption that the block thickness is infinite. Note that Wright and Ockendon, and Bai did not find the infimum of $2\pi/\xi_m(t_0)$. Batra and Chen [17–20] extended Wright and Ockendon's and Molinari's work on SBS to strain-rate gradient-dependent materials deformed in simple shear, and gave approximate analytical expressions for the critical wavelength for heat-conducting nonpolar materials and locally adiabatic deformations of strain-rate gradient-dependent materials. It was found that the material characteristic length and heat conduction play important roles in the SBS. An interesting result derived by Batra and Chen is that the SBS is finite even in locally adiabatic deformations of strain-rate

gradient-dependent materials. They have scrutinized the effect of material parameters, microstructural variables, and different thermoviscoplastic relations on the SBS and the instability strain.

Batra and Wei [21] recently obtained a closed-form expression for the SBS for a strain hardening, strain-rate hardening and thermally softening thermoviscoplastic material deformed in simple shear. Xue et al. [10] have shown that the Grady–Kipp [11], the Wright–Ockendon [15] and the Molinari [16] models do not predict well the SBS in titanium alloys. They proposed that the rate of initiation, the rate of growth and the characteristic time of interaction between shear bands be considered. The work presented herein shows that the geometric softening/hardening due to the change in the area of cross-section of a bar deformed in simple tension/compression has a significant effect on the SBS.

Here we use the perturbation method to find the instability strain and the SBS for a heat-conducting, strain hardening, strain-rate hardening, and thermally softening material deformed in simple tension/compression. The softening of the material due to damage evolution and the change in the cross-section is also considered. A major difference between this work and the earlier ones dealing with simple shearing deformations is the geometric softening/hardening induced by the change in the cross-sectional area. It is found that in the absence of heat conduction, the perturbation method and the Considerè criterion give the same value of the instability strain; this is true even when inertia, thermal softening and damage evolution are considered. The dependence of the instability strain and the SBS on material parameters is delineated. Scaling laws for the SBS are closely examined.

2. Governing equations

We study one-dimensional thermomechanical deformations of a homogeneous, isotropic, strain hardening, strain-rate hardening, thermally softening and damage softening thermoviscoplastic body deformed in simple tension/compression. Equations describing deformations are

$$A\rho\frac{\partial v}{\partial t}=\frac{\partial(A\sigma)}{\partial x},\quad A\rho c\frac{\partial\theta}{\partial t}=\beta A\sigma\frac{\partial\varepsilon}{\partial t}+\lambda\frac{\partial}{\partial x}\left(A\frac{\partial\theta}{\partial x}\right),$$
$$\sigma=\sigma(\varepsilon,\dot{\varepsilon},\theta,\phi_1,\phi_2,\ldots,\phi_n),\quad \frac{\mathrm{d}\phi_i}{\mathrm{d}\varepsilon}=f_i(\sigma,\varepsilon,\dot{\varepsilon},\theta,\phi_1,\phi_2,\ldots,\phi_n),\quad i=1,2,\ldots,n. \tag{1}$$

Here, ρ is the mass density, v the axial velocity of a material particle, t the time, σ the axial Cauchy stress, ε the axial strain, λ the thermal conductivity, c the specific heat, θ the temperature rise, β the Taylor–Quinney factor describing the fraction of plastic working converted into heating, and A is the cross-sectional area of the bar. Usually, $0.85\leqslant\beta\leqslant0.95$. Elastic deformations have been neglected because they are very small as compared to the plastic deformations. Eqs. $(1)_1$ and $(1)_2$ express, respectively, the balance of linear momentum and the balance of internal energy. Eq. $(1)_3$ gives the constitutive relation expressing the flow stress as a function of strain, strain rate, temperature and internal variables whose evolution is given by Eq. $(1)_4$. Internal variables ϕ_i are associated with various dissipative mechanisms; each ϕ_i may be a scalar, a vector or a tensor, and n is a sufficiently large number to fully characterize the material. An internal variable is nonobservable and is obtained from an evolution law. Since the treatment of n damage variables is similar to that of one variable, henceforth we set $n=1$ and denote the damage variable by ϕ. Lateral inertia effects which could cause surface instability have been neglected for simplicity. The system of Eqs. (1) is similar to that employed by Batra and Kim [22] to analyze simple shearing deformations of a block of varying thickness except that they do not consider the damage variable ϕ and did not study the stability of solutions and the SBS. Batra and Chen [18] have delineated the effect of microstructural (or internal) parameters on the SBS in a thermoviscoplastic material deformed in simple shear.

We define the axial strain ε as

$$\varepsilon=\ln(L/L_0), \tag{2}$$

where L_0 and L are the undeformed and the deformed lengths of the bar. Following the usual assumption that plastic deformations are isochoric, an alternative expression for ε is

$$\varepsilon=\ln(A_0/A),\quad A=A_0\exp(-\varepsilon). \tag{3}$$

Here we have neglected the effect of damage, if any, on the change in volume. For isochoric deformations of a homogeneous body the mass density is a constant. Substituting for A from Eq. $(3)_2$ into Eq. $(1)_1$ and eliminating $A_0\exp(-\varepsilon)$ we get

$$\rho\frac{\partial v}{\partial t}=\frac{\partial \sigma}{\partial x}-\sigma\frac{\partial \varepsilon}{\partial x}. \tag{4}$$

Differentiating both sides of Eq. (4) with respect to x and using $\partial\varepsilon/\partial t=\partial v/\partial x$ we obtain

$$\rho\frac{\partial^2\varepsilon}{\partial t^2}=\frac{\partial^2\sigma}{\partial x^2}-\left(\frac{\partial\sigma}{\partial x}\frac{\partial\varepsilon}{\partial x}+\sigma\frac{\partial^2\varepsilon}{\partial x^2}\right). \tag{5}$$

Similarly, the energy balance equation $(1)_2$ can be simplified to

$$\beta\sigma\frac{\partial\varepsilon}{\partial t}=\rho c\frac{\partial\theta}{\partial t}-\lambda\left(\frac{\partial^2\theta}{\partial x^2}-\frac{\partial\varepsilon}{\partial x}\frac{\partial\theta}{\partial x}\right). \tag{6}$$

The term in parentheses on the right-hand side of Eq. (5) and the third term on the right-hand side of Eq. (6) are due to the change in the area of cross-section of the bar.

3. Instability strain derived from the perturbation method

We assume that the bar is of infinite length; thus, admissible perturbations need not satisfy boundary conditions at the end sections. The analysis presented in this section closely follows Bai's work [14] on simple shearing deformations. However, the effect of geometric softening/hardening in the simple tension/compression of a bar introduces additional terms.

Let $\mathbf{S}^0(t)\equiv(\varepsilon^0(t),\sigma^0(t),\theta^0(t),\phi^0(t))$ be a solution of Eqs. (5) and (6) corresponding to homogeneous deformations of the bar, and $\delta\mathbf{S}(t_0,x,t)$ with $|\delta\mathbf{S}(t_0,x,t)|\ll|\mathbf{S}(t_0)|$ denote an infinitesimal perturbation in $\mathbf{S}^0(t_0)$. Perturbations considered are such that $\mathbf{S}^0(t_0)+\delta\mathbf{S}(t_0,x,t)$ satisfies Eqs. (5) and (6), and

$$\delta\mathbf{S}=\delta\mathbf{S}^0e^{i\xi x}e^{\eta(t-t_0)}, \tag{7}$$

where $\delta\mathbf{S}^0$ is the amplitude of the perturbation, ξ the wave number in units of 1/length, and η equals the growth rate of the perturbation at time t_0. $\mathrm{Re}(\eta)>0$ implies that perturbations will grow signifying the instability of the homogeneous solution at time t_0; otherwise it is stable. We assume that perturbations of all wave numbers are admissible.

Eq. $(1)_3$ implies that

$$\delta\sigma=(Q_0+\eta R_0)\delta\varepsilon-P_0\delta\theta+Y_0\delta\phi, \tag{8}$$

where

$$P_0=-\left.\frac{\partial\sigma}{\partial\theta}\right|_{\mathbf{s}=\mathbf{s}^0},\quad Q_0=\left.\frac{\partial\sigma}{\partial\varepsilon}\right|_{\mathbf{s}=\mathbf{s}^0},\quad R_0=\left.\frac{\partial\sigma}{\partial\dot\varepsilon}\right|_{\mathbf{s}=\mathbf{s}^0},\quad Y_0=\left.\frac{\partial\sigma}{\partial\phi}\right|_{\mathbf{s}=\mathbf{s}^0}. \tag{9}$$

Thus, P_0 equals thermal softening of the material, Q_0 its strain hardening, R_0 strain-rate hardening, and Y_0 a thermodynamic force conjugate to the internal variable ϕ. Note that

$$P_0\geqslant 0,\quad Q_0\geqslant 0\quad\text{and}\quad R_0\geqslant 0. \tag{10}$$

In terms of nondimensional variables

$$\bar\eta=\frac{\lambda\eta}{cQ_0},\quad \bar\xi=\frac{\lambda\xi}{c\sqrt{\rho Q_0}},\quad I=\frac{cR_0}{\lambda},\quad J=\frac{\beta\sigma^0P_0-\rho c(Y_0f^0-\sigma^0)}{\rho cQ_0},$$
$$\Gamma=\frac{\beta\lambda P_0\dot\varepsilon_0}{\rho c^2Q_0},\quad E=1-\frac{(Y_0f^0)-\sigma^0}{Q_0},\quad F=\frac{\beta\lambda P_0\dot\varepsilon_0\sigma^0}{\rho c^2Q_0^2},$$

where $f^0 = \partial\phi/\partial\varepsilon|_{\mathbf{s}=\mathbf{s}^0}$, and $\dot{\varepsilon}_0$ is the nominal axial strain rate, we get the following equation for the determination of $\bar{\eta}$:

$$\bar{\eta}^3 + [\Gamma + (1+I)\bar{\xi}^2]\bar{\eta}^2 + (I\bar{\xi}^2 + 1 - J)\bar{\xi}^2\bar{\eta} + (E\bar{\xi}^4 - F\bar{\xi}^2) = 0. \tag{11}$$

The third and fourth terms on the left-hand side of Eq. (11) differ from the third and fourth terms of Eq. (15) of [21] and account for the differences in results for simple shearing and simple tensile deformations (for simple shearing deformations, $E = 1$, $F = 0$, $J = \beta\sigma^0 P_0/(\rho c Q_0)$).

For given values of t_0 and $\bar{\xi}$, Eq. (11) has three roots; the root with the largest positive real part will make the homogeneous solution most unstable. For very short wavelengths, $\bar{\xi} \to \infty$, Eq. (11) has the solution $\bar{\eta} = -E/I$ which in the absence of internal variables is negative provided that $\sigma^0 \geqslant 0$. For extremely long wavelengths, $\bar{\xi} \to 0$, $\bar{\eta} \to 0$ and $-\Gamma$. If $\bar{\eta} \to 0$ from above, then the simple tensile deformations are unstable for perturbations of very long wavelengths, and the growth rate of the perturbed solution decreases with an increase in the wavelength of perturbations. Thus, the tensile deformation is stable with respect to disturbances of infinitesimal wavelengths, but may be unstable with respect to disturbances of finite wavelengths. We seek the wave number $\bar{\xi}_m$ for which $\bar{\eta}$ has the maximum value $\bar{\eta}_m$. Thus, $\bar{\eta}_m$ and $\bar{\xi}_m$ satisfy Eq. (11) and

$$\left(\frac{\mathrm{d}\bar{\eta}}{\mathrm{d}\bar{\xi}^2}\right)\Bigg|_{(\bar{\eta}=\bar{\eta}_m, \bar{\xi}=\bar{\xi}_m)} = 0. \tag{12}$$

Eqs. (11) and (12) give

$$4\bar{\eta}_m^2(\Gamma + \bar{\eta}_m)(I\bar{\eta}_m + E) = [F + (J-1)\bar{\eta}_m - (I+1)\bar{\eta}_m^2]^2. \tag{13}$$

It should be noted that $\bar{\eta}_m = 0$ is not a solution of Eq. (13) while the instability criterion is usually obtained by setting $\bar{\eta}_m = 0$, e.g., see [14].

Even though known imprecisely, orders of magnitude of different material parameters can be estimated. For example, approximate values of thermophysical parameters for most metals are:

$$\rho \sim 10^3\,\mathrm{kg/m^3}, \quad \sigma^0 \sim 10^9\,\mathrm{kg/ms^2}, \quad \dot{\varepsilon} \sim 10^3/\mathrm{s}, \quad c \sim 10^3\,\mathrm{J/kg\,K}, \quad \lambda \sim 10^2\,\mathrm{W/mK},$$
$$P_0 \sim 10^6\,\mathrm{kg/ms^2\,K}, \quad Q_0 \sim 10^9\,\mathrm{kg/ms^2}. \tag{14}$$

Hence, $F \simeq 10^{-4}$ and terms involving F play a negligible role and will be disregarded. With $F = 0$, $\bar{\eta}_m = 0$ satisfies Eq. (13), and its largest root is

$$\bar{\eta}_m = \frac{2[(I+1)(J-1) + 2(E + I\Gamma)] + \sqrt{4[(I+1)(J-1) + 2(E+I\Gamma)]^2 - [(J-1)^2 - 4\Gamma E]}}{2(I-1)^2}. \tag{15}$$

The instability criterion obtained by setting $\bar{\eta}_m = 0$ is

$$J = 1 + 2\sqrt{\Gamma E}. \tag{16}$$

For locally adiabatic deformations, $\lambda = 0$, and Eq. (16) yields the following instability criterion:

$$J = 1, \quad \text{or} \quad \beta\sigma^0 P_0 - \rho c(Y_0 f^0 - \sigma^0) = \rho c Q_0. \tag{17}$$

Eq. (17) states that for locally adiabatic deformations instability occurs when the combined effects of softening caused by the decrease of cross-section of the bar, damage evolution and heating due to plastic working overcome work hardening of the material. Eq. (17) is the same as the Considerè's condition: $\mathrm{d}\sigma/\mathrm{d}\varepsilon = \sigma$. In the absence of internal variables (i.e. $Y_0 = 0$) the instability criterion (17) differs from that ($\beta\sigma^0 P_0/(\rho c Q_0) = 1$) in the simple shearing deformations due to the change in the area of cross-section.

4. Shear band spacing

Substitution for $\bar{\eta}_m$ from Eq. (15) into Eq. (13), and setting $F = 0$ give

$$b_1\bar{\xi}_m^4 + b_2\bar{\xi}_m^2 + b_3 = 0, \tag{18}$$

where

$$b_1 = (I-1)^2[E(I+1) - I(1-J)],$$
$$b_2 = 2\{2I(1-J)^2 - (I+1)(1-J)(3E + I\Gamma) + 2E[\Gamma I^2 + \Gamma + 2E]\},$$
$$b_3 = [4\Gamma E - (1-J)^2][\Gamma(I+1) - (1-J)]. \tag{19}$$

A positive root of Eq. (18) is

$$\bar{\xi}_m^2 = \frac{-b_2 + \sqrt{b_2^2 - 4b_1 b_3}}{2b_1}. \tag{20}$$

For a strain-rate-independent material, $R_0 = 0$, $I = 0$, and we get

$$\bar{\xi}_m^2 = \frac{(1+N)[(1+N) + (2\Gamma + 3M)] + [3(N+1) + M]\sqrt{(M+\Gamma)(1+N)}}{(1+N)}, \tag{21}$$

where

$$M = \frac{(\beta P_0 + \rho c)\sigma^0}{\rho c Q_0}, \quad N = \frac{Y_0 f^0}{Q_0}. \tag{22}$$

For most materials deformed at high strain rates, $\Gamma \ll M$, and Eq. (21) reduces to

$$\bar{\xi}_m^2 = \frac{(1+N)[(1+N) + 3M] + [3(N+1) + M]\sqrt{M(1+N)}}{(1+N)}. \tag{23}$$

If the effect of internal variables is neglected, then

$$\bar{\xi}_m^2 = 1 + 3M + (3+M)\sqrt{M}. \tag{24}$$

For $M \gg 1$,

$$\bar{\xi}_m \simeq M^{3/4} = \left[\frac{\sigma^0}{Q_0}\left(1 + \frac{\beta P_0}{\rho c}\right)\right]^{3/4}. \tag{25}$$

According to Wright and Ockendon's [15] postulate, the wavelength of the dominant instability mode with the maximum initial growth rate at the prescribed strain or time determines the SBS L_s. That is,

$$L_s = 2\pi/\xi_m(t_0) \simeq \frac{2\pi\lambda}{c}\left(\frac{Q_0}{\rho^2\sigma^{03}}\right)^{1/4}\left(1 + \frac{\beta P_0}{\rho c}\right)^{-3/4}, \tag{26}$$

where we have used Eq. (25) and the relationship between $\bar{\xi}$ and ξ. However, Molinari's definition

$$L_s = \inf_{t_0 \geqslant 0}(2\pi/\xi_m(t_0)) \tag{27}$$

will give the least possible spacing between adjacent shear bands. Substitution for ξ_m from Eq. (25) into Eq. (27) gives the SBS for a strain-rate-independent material. For a strain-rate-dependent material Eq. (20) and either Eq. (26) or Eq. (27) give the SBS.

5. Damage evolution equation

From Rice and Tracey's [22] growth law of a single void in a perfectly plastic media and Bai et al.'s [23,24] conservation equation for ideal cracks, Wei and Batra [25] derived the following equation for the damage evolution induced by the growth of existing voids:

$$\dot{\phi} = 0.566 \exp^{[(\sigma_{kk}/2\sigma_y)]}\dot{\varepsilon}\phi H(\sigma_{kk} - 0). \tag{28}$$

Here, σ_y approximately equals the flow stress, H is the Heaviside step function, $\sigma_{kk} = (\sigma_{11} + \sigma_{22} + \sigma_{33})$, and a superimposed dot indicates the material time derivative. Eq. (28) implies that the damage grows only when the hydrostatic stress, $\sigma_{kk}/3$, is tensile; otherwise its value remains unchanged. Higher values of the triaxiality

factor, (σ_{kk}/σ_y), increase the growth rate of damage. On the assumption that σ_{kk}/σ_y is nearly constant we can integrate Eq. (28) to obtain

$$\phi = \phi_0 \exp(k\varepsilon) H(\sigma_{kk} - 0), \quad k = 0.566 \exp\left(\frac{\sigma_{kk}}{2\sigma_y}\right), \tag{29}$$

where ϕ_0 is the initial damage. For our problem $\sigma_{kk}/2\sigma_y = 1/2$ since deformations prior to the onset of necking have been considered, and $\sigma_{22} = \sigma_{33} = 0$. Thus, Eq. (29) simplifies to $\phi = \phi_0 \exp(0.933\varepsilon)\ H(\sigma_{kk} - 0)$.

6. Constitutive relation and the related instability criterion

We use the following constitutive relation:

$$\sigma = \sigma_0 \left(1 + \frac{\varepsilon}{\varepsilon_y}\right)^n (1 + b\dot{\varepsilon})^m \left(\frac{\theta_m - \theta}{\theta_m - \theta_r}\right)^v (1 - \phi)^q \tag{30}$$

for studying the effect of different parameters on the SBS. Here, m and n are, respectively, the strain- and the strain-rate hardening exponents; ε_y and n characterize the strain hardening of the material, b and m its strain-rate hardening, θ_m is the melting temperature, θ_r the room temperature, and v the thermal softening exponent. The factor $(1 - \phi)^q$ accounts for material softening due to damage evolution; $\phi = 0$ corresponds to the undamaged material and $\phi = 1$ to totally damaged material. Henceforth we assume that the bar is deformed at a constant axial strain rate $\dot{\varepsilon}_0$. Prior to perturbing the homogeneous solution, the temperature is uniform in the body, $\phi = 0$ and there is no heat conduction. Thus, for homogeneous deformations, we can set $k = 0$ and compute the temperature by substituting for σ from Eq. (30) into Eq. $(1)_2$, and integrating the resulting equation. The result is

$$\theta = \theta_m - (\theta_m - \theta_r) \exp\left\{ - \frac{\beta \sigma_0 \varepsilon_y (1 + b\dot{\varepsilon}_0)^m}{\rho c (\theta_m - \theta_r)(n+1)} \left[\left(1 + \frac{\varepsilon}{\varepsilon_y}\right)^{n+1} - 1 \right] \right\}, \quad v = 1,$$

$$\theta = \theta_m - \left\{ (\theta_m - \theta_r)^{1-v} - \frac{\beta(1-v)\sigma_0 \varepsilon_y (1 + b\dot{\varepsilon}_0)^m}{\rho c (\theta_m - \theta_r)^v (1+n)} \left[\left(1 + \frac{\varepsilon}{\varepsilon_y}\right)^{n+1} - 1 \right] \right\}^{1/(1-v)} \quad \text{for } v \neq 1. \tag{31}$$

For a bar deformed at a constant axial strain rate, the instability criterion (17) becomes

$$\frac{n}{\varepsilon_y + \varepsilon} - \frac{v}{\theta_m - \theta} \frac{d\theta}{d\varepsilon} - \frac{q}{1 - \phi} \frac{d\phi}{d\varepsilon} = 1. \tag{32}$$

Values of $d\theta/d\varepsilon$ and $d\phi/d\varepsilon$ can be obtained from Eqs. (31) and (29), respectively.

7. Results and discussion

During the computation of results, we have assumed that the bar is made of HY-100 steel and assigned following values to various material parameters:

$$\begin{aligned} &\sigma_0 = 702\,\text{MPa}, \quad n = 0.107, \quad m = 0.0117, \quad \rho = 7860\,\text{kg/m}^3, \quad c = 473\,\text{J/kg K}, \\ &\varepsilon_y = 0.007, \quad \beta = 0.9, \quad \dot{\varepsilon}_0 = 1000/\text{s}, \quad \theta_m = 1500\,\text{K}, \quad \theta_r = 300\,\text{K}, \quad b = 17\,320\,\text{s}, \\ &\lambda = 49.73\,\text{W/m}^2\,\text{K}, \quad \phi_0 = 0.0, \quad q = 1, \quad v = 1. \end{aligned} \tag{33}$$

Since $b\dot{\varepsilon} \gg 1$ and $m \ll 1$, therefore $(1 + b\dot{\varepsilon})^m \simeq b^m \dot{\varepsilon}^m$, and m equals the strain-rate hardening exponent. Similarly, for $\varepsilon \simeq 0.1$, $\varepsilon/\varepsilon_y \simeq 14$, $(1 + \varepsilon/\varepsilon_y)^n \simeq (\varepsilon/\varepsilon_y)^n$, and n equals the strain hardening exponent. While performing parametric studies, only one of these parameters is varied. For different values of the axial strain rate, Fig. 1 depicts the axial stress vs. the axial strain curves as computed from Eq. (30). Deformations are assumed to be locally adiabatic at axial strain rates of 10^3/s and higher, and isothermal at strain rates of 10^{-4} and 10^{-6}/s. For locally adiabatic deformations the temperature rise is computed from Eq. $(31)_1$. The curves in Fig. 1 do not include the effect of inertia forces. As expected, the axial stress is a monotonically increasing function of the axial strain for isothermal deformations. However, for locally adiabatic deformations the axial stress peaks

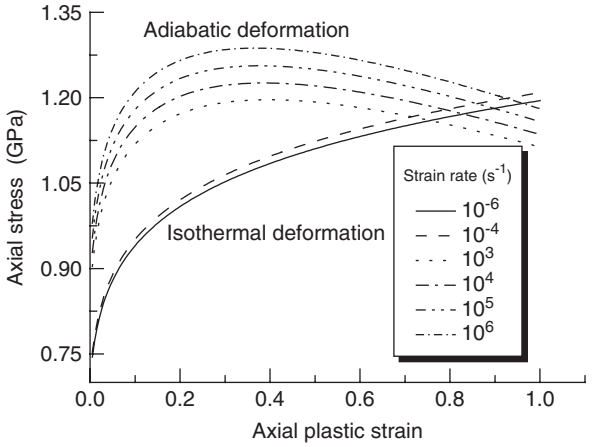

Fig. 1. Axial stress vs. axial plastic strain curves for axial tensile deformations of a HY-100 steel at various strain rates.

and the value of this peak stress increases monotonically with an increase in the axial strain rate. The axial plastic strain corresponding to the peak in the axial stress decreases slowly with an increase in the axial strain rate.

7.1. Instability strain

Fig. 2a–e evinces the dependence of the instability strain, computed from Eq. (32), upon the axial strain-rate $\dot{\varepsilon}_0$, the strain-rate hardening exponent m, the strain hardening exponent n, the thermal softening exponent ν, and the initial damage ϕ_0. The instability strain computed from Eq. (32) is considerably smaller than the strain at which an adiabatic shear band initiates, e.g., see [26] who studied numerically plane strain tensile deformations of a thermoviscoplastic body. A bar usually fractures after a shear band has developed. Because of the log scale along the horizontal axis in Fig. 2a, the instability strain decreases affinely with an increase in the log (average axial strain rate). However, the rate of decrease is rather small since the instability strain drops from 8.0% at $\dot{\varepsilon}_0 = 10^3/\text{s}$ to 7.9% at $\dot{\varepsilon}_0 = 10^6/\text{s}$. For all practical purposes, it may be taken to equal 8% for $10^3/\text{s} \leqslant \dot{\varepsilon}_0 \leqslant 10^6/\text{s}$. Similarly, when the strain-rate hardening exponent is increased by a factor of 5, the instability strain decreases affinely from 8.2% for $m = 0.00468$ to 7.7% for $m = 0.0234$. For a similar proportional increase in the value of the strain hardening exponent n, the instability strain increases from 2.9% to 15.3% or by a factor of ~5. Thus, the dependence of the instability strain upon the strain hardening exponent is much stronger than that on the strain-rate hardening exponent.

Results plotted in Fig. 2d also reveal the effect of the geometric softening. For $\nu = 0$, there is no thermal softening and the instability occurs only due to geometric softening. Thus, the influence of additional softening due to heating decreases the instability strain from 10% for $\nu = 0$ to about 6.7% for $\nu = 2$. Note that for an axial strain of 10%, the temperature rises by about 19 K. Results plotted in Fig. 2e suggest that the instability strain decreases very slowly from 8.0% for $\phi_0 = 0$ to 7.7% for $\phi_0 = 0.04$. For $\phi_0 = 0$, $\phi = 0$ and there is no evolution of damage. Results of Fig. 2a–e agree qualitatively with those for the simple shearing problem. For plane strain tensile deformations of a steel prismatic body modeled as a thermoviscoplastic material and deformed at a nominal axial strain rate of 5000/s, Batra and Lear [26] found that the structure became unstable at axial strains of 4.9% and 4.85% according to the Considerè and the Hart criteria, respectively.

In order to vividly delineate the effect of geometric softening/hardening, we have plotted in Fig. 2f the variation of the instability strain with the axial strain rate both with and without the effects of geometric softening. For each case the strain rate does not affect much the instability strain. It is transparent that the geometric softening has a significant effect on the instability strain. For an axial strain rate of $10^3/\text{s}$ the instability strain decreases from ~39.6% in the absence of geometric softening to ~8% when geometric softening effects are considered. To reinforce this effect we have plotted in Fig. 2g the dependence of the

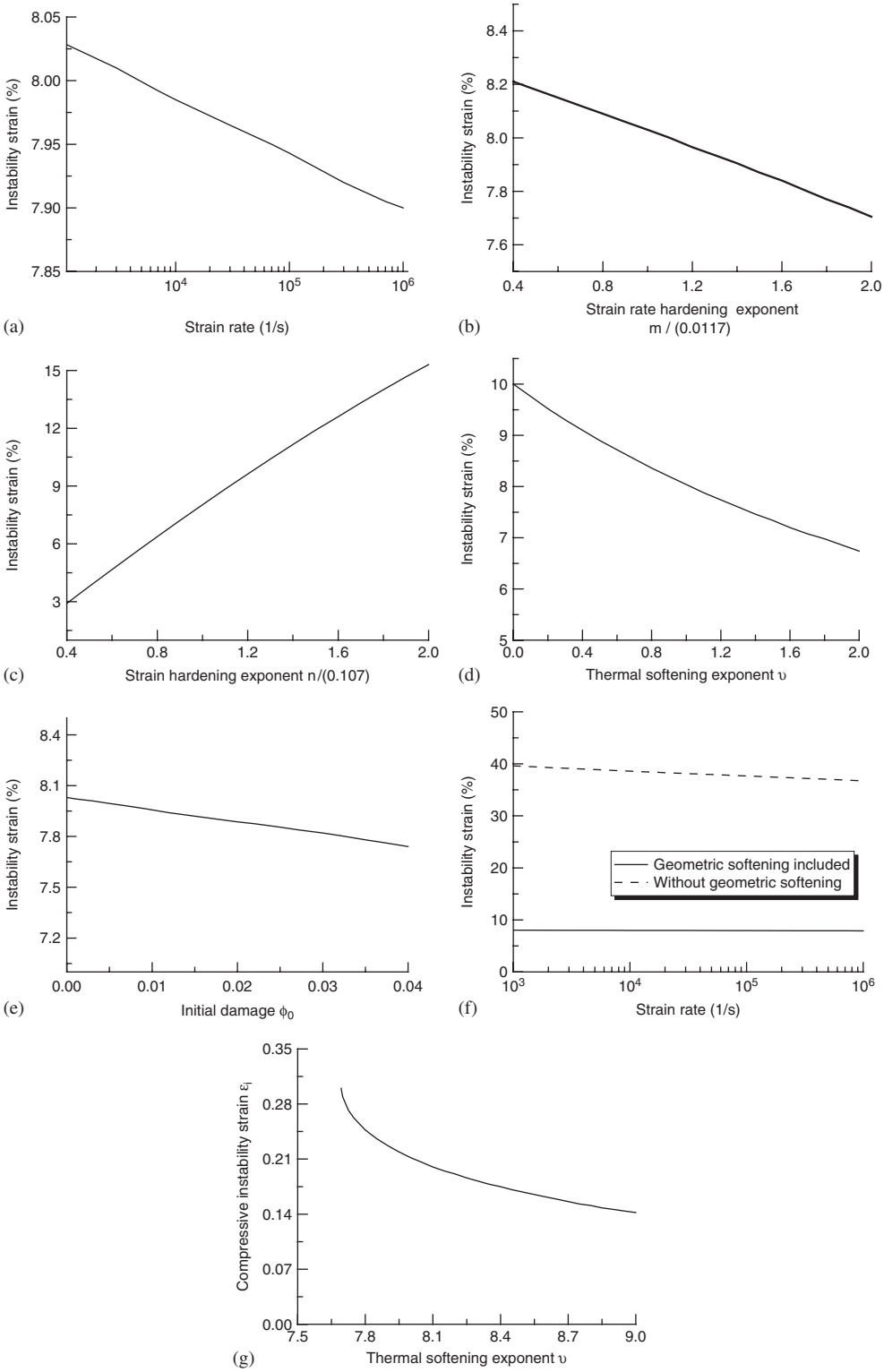

Fig. 2. The dependence of the instability strain upon (a) the axial strain rate, (b) the strain-rate hardening exponent, (c) the strain hardening exponent, (d) the thermal softening exponent, (e) the initial damage and (f) with and without geometric softening. Results plotted in (g) are for axial compressive deformations.

instability strain upon the thermal softening exponent v for axial compressive deformations. It is found that in compression the instability occurs at a much higher value of v than that in tension. Even then, the instability strain for compressive deformations is noticeably higher than that for tensile deformations. For normal values of v, the instability strain in compression is incredibly large because of the dominant geometric hardening. One may not observe such high axial compressive strains experimentally because of the presence of material defects and/or frictional forces between the loading device and the specimen.

7.2. Shear band spacing

7.2.1. SBS according to the Wright–Ockendon criterion

For several values of the uniform axial strain rate, Fig. 3a exhibits the maximum initial growth rate of the perturbation as a function of the axial strain when the homogeneous solution is perturbed. Recall that the instability strain equals ~0.08 for the simple tensile deformations. The SBS, computed from the Wright and Ockendon relation (26), i.e., $L_s = 2\pi/\xi_m(t_0)$, is plotted in Fig. 3b. It is clear that for the homogeneous solution perturbed at the same value of the axial strain the SBS decreases monotonically with an increase in the axial strain rate. For a fixed axial strain rate, the SBS is essentially unchanged if the homogeneous solution is perturbed at an axial strain greater than 0.5. If the perturbation is introduced at an axial strain of 0.25, the SBS equals ~26.8, 4.8, 0.86, 0.15 and 0.03 mm for $\dot{\varepsilon}_0 = 10^1,\ 10^2,\ 10^3,\ 10^4$ and 10^5/s, respectively. Thus, the SBS strongly depends upon the axial strain rate. These results imply that the SBS $\propto (\dot{\varepsilon}_0)^{-0.75}$. We note that for the simple shearing deformations studied in [21], the SBS $\propto$ (nominal shear strain rate)$^{-0.787}$; the exponents -0.75 and -0.787 for the two types of deformations are close to each other. Results plotted in Fig. 4a,b illustrate that the initial damage influences the maximum initial growth rate and the SBS only if the homogeneous solution is perturbed at a rather large value of the axial strain.

In order to clearly delineate the effect of geometric softening on the SBS we also computed results by neglecting the third term on the right-hand side of Eq. (6) and the term in parentheses on the right-hand side of Eq. (5). It is equivalent to assuming that the cross-section of the bar is a constant or neglecting lateral deformations. Eqs. (5) and (6) then reduce to those for a simple shearing problem. Fig. 5a,b exhibits the maximum initial growth rate of a perturbation and the corresponding SBS computed from Eq. (26). It is clear that the consideration of geometric softening strongly influences the SBS and the maximum initial growth rate of perturbation. As expected, with geometric softening perturbations introduced at a small value of the effective plastic strain grow rapidly. For $\varepsilon_0 \geqslant \sim 0.4$, the consideration of geometric softening decreases the SBS as compared to that without the geometric softening effect. However, in each case the SBS $\propto \dot{\varepsilon}_0^{-0.76}$ as should be evident from the results exhibited in Fig. 5c. Table 1 lists values of the SBS for nominal axial strain rates of 10^3, 10^4 and 10^5/s with and without the effects of geometric softening.

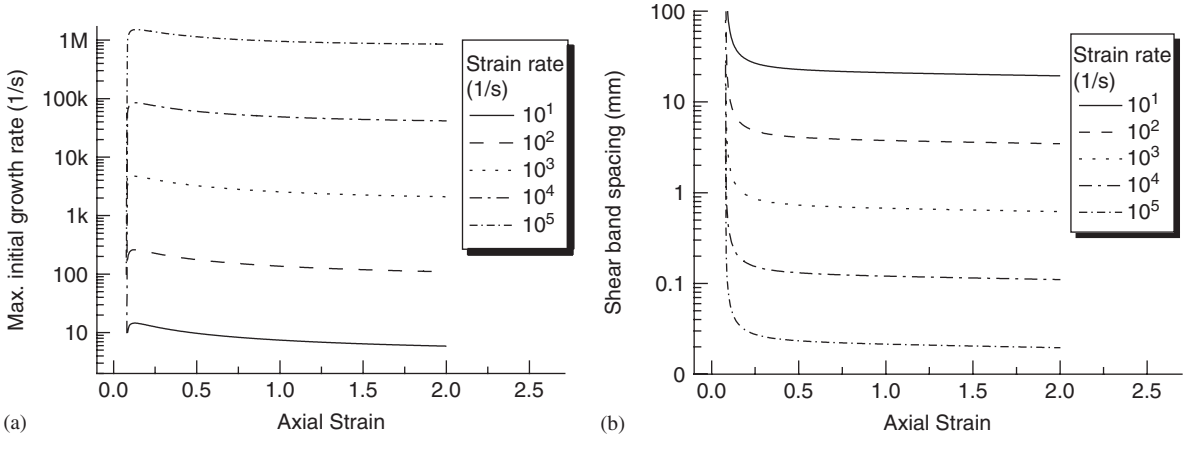

Fig. 3. For five values of the axial strain rate, dependence upon the axial strain when the homogeneous solution is perturbed of (a) the maximum initial growth rate and (b) the shear band spacing.

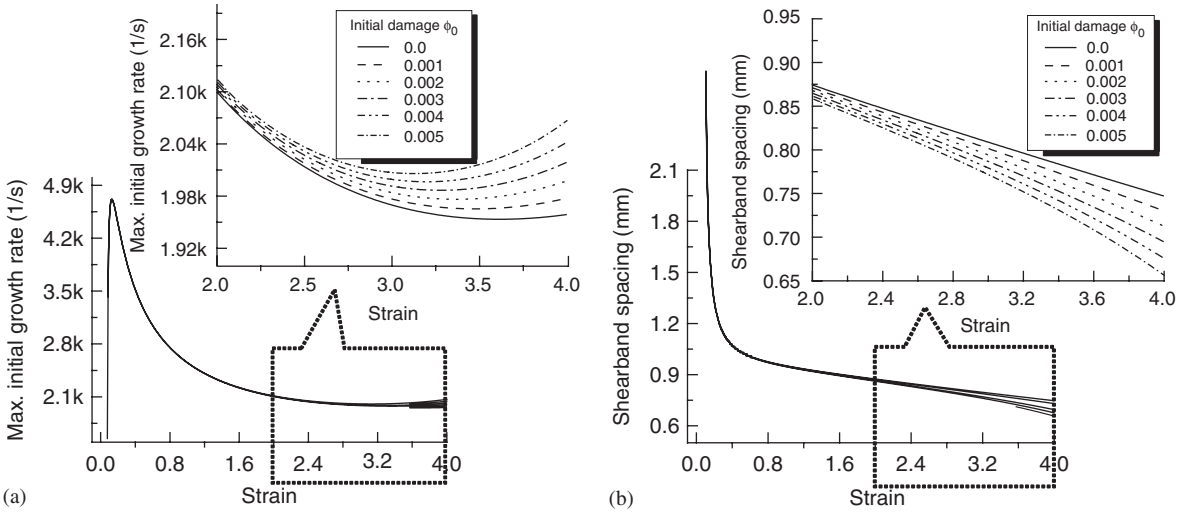

Fig. 4. For six values of the initial damage, dependence upon the axial strain when the homogeneous solution is perturbed of (a) the maximum initial growth rate and (b) the shear band spacing.

7.2.2. SBS according to the Molinari criterion

Results computed with Molinari's definition of the SBS do not depend upon the axial strain when the homogeneous solution is perturbed. Fig. 6a–i exhibits the SBS, L_s, as a function of the axial strain rate $\dot{\varepsilon}_0$, the thermal conductivity λ, the Taylor–Quinney parameter β, the specific heat c, the strain-rate hardening exponent m, the strain hardening exponent n, and the thermal softening exponent v. The plot in Fig. 6a gives $L_s \propto \dot{\varepsilon}_0^{-0.757}$. It is interesting to note that the exponent -0.757 obtained here for strain hardening and geometrically softening material is very close to the -0.75 obtained in [15,16] for non-strain-hardening materials deformed in simple shear, and -0.787 obtained in [21] for a strain hardening material deformed in simple shear.

When the dependence of L_s upon λ is written as $L_s \propto \lambda^{\bar{\chi}}$, then we conclude from the plots in Fig. 6b that $\bar{\chi} = 0.188$, 0.218, 0.233, 0.242 and 0.242 for $m/0.0117 = 0.001$, 0.01, 0.1, 1.0 and 2.0, respectively. Thus, for $m = 0.0117$ and 0.0234, $L_s \propto \lambda^{0.242}$ which agrees with $\lambda^{0.25}$ derived in [15,16,21] for simple shearing deformations. However, for small values of $m/0.0117$, $\bar{\chi}$ is not a constant but varies between 0.188 and 0.233. For simple shearing deformations Batra and Wei [21] found that $\bar{\chi} \simeq 0.5$ for $m \simeq 10^{-6}$. Thus, the dependence of L_s upon the thermal conductivity is quite different for simple tensile deformations as compared to that for simple shearing deformations. We note that the third term on the right-hand side of Eq. (6) involving the product of thermal conductivity with the spatial gradients of ε and θ is missing in the simple shearing problem.

From the plot of $\log(L_s)$ vs. β given in Fig. 6c one concludes that there is no scaling law for L_s vs. β; it was verified by plotting $\log(L_s)$ vs. $\log(\beta)$. Whereas, $\log(L_s)$ decreases slowly with an increase in β for small values of m, $\log(L_s)$ increases gradually with an increase in β for large values of m. For simple shearing deformations it was found in [21] that $L_s \propto \beta^{\chi_\beta}$ where $-0.5 \leqslant \chi_\beta \leqslant -0.44$ for several combinations of values of m and n.

Fig. 6d illustrates on a log–log plot the variation of the SBS, L_s, with the specific heat c. When written as $L_s \propto c^{\hat{\chi}}$, the value of $\hat{\chi}$ depends upon the strain-rate hardening exponent m; it increases monotonically with an increase in the value of m. Furthermore, $\hat{\chi}$ is nearly zero for small values of m but is negative for $m/0.0117 \geqslant 0.001$. For simple shearing deformations $\hat{\chi}$ depends upon m and n, and $-0.2 \leqslant \hat{\chi} \leqslant 0.3$. There appears to be no scaling law for the dependence of the SBS upon the specific heat.

Results plotted in Fig. 6e reveal that for a fixed value of $n/0.107$ the SBS increases monotonically with an increase in the strain-rate hardening exponent m. For $n = 0.0107$ and 0.107 the SBS increases linearly with m; the positive intercept of the line with the y-axis is obscured by the scale used to plot L_s. The plots of $\log(L_s)$ vs. the strain hardening exponent n given in Fig. 6f suggest that $\log(L_s)$ is virtually independent of the strain hardening exponent n for $0 < n/0.107 < 2.5$ but the value of $\log(L_s)$ strongly depends upon the strain-rate

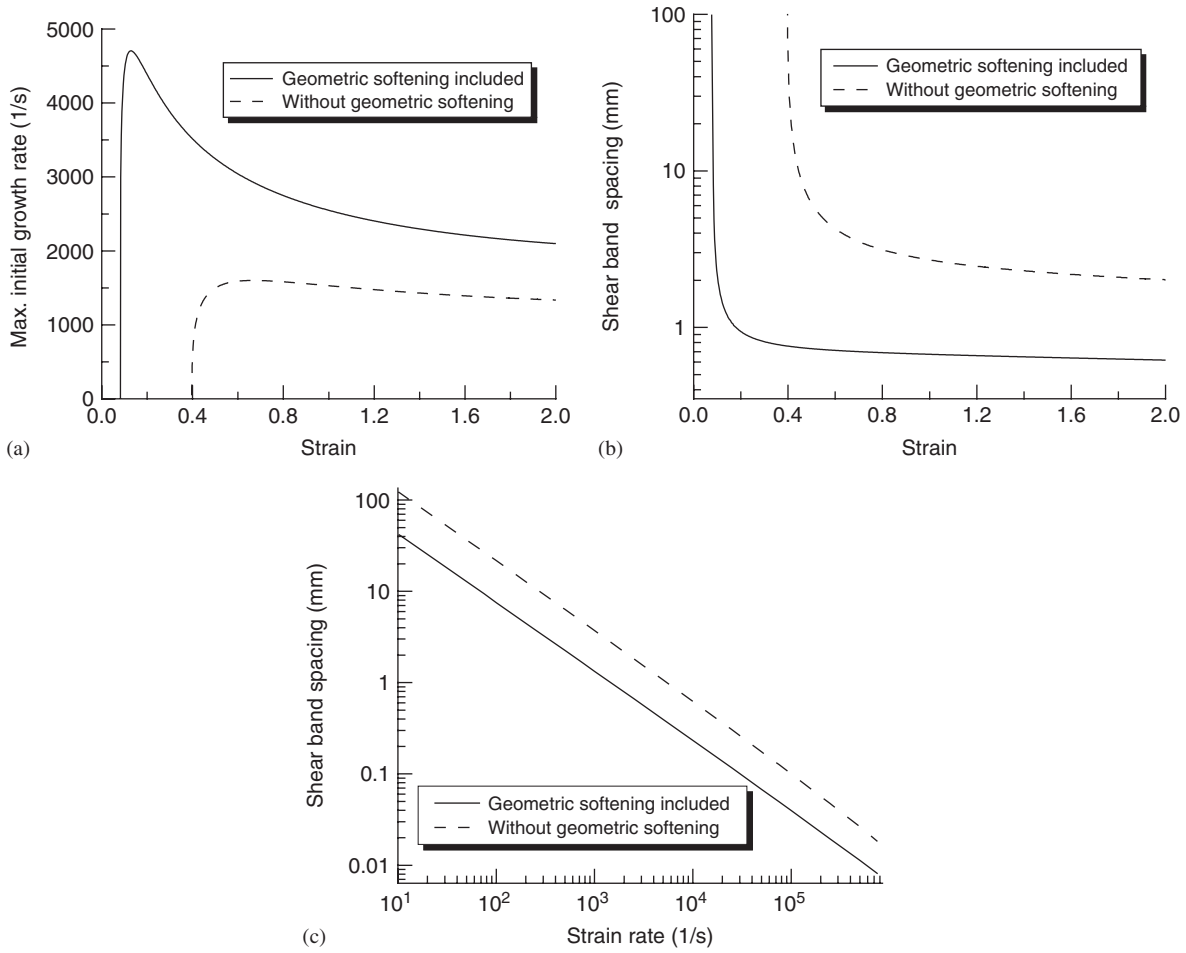

Fig. 5. For an axial strain rate of 1000/s, dependence upon the axial strain when the homogeneous solution is perturbed of (a) the maximum initial growth rate, and (b) the shear band spacing and (c) for an axial strain of 0.4, dependence of the shear band spacing upon the axial strain rate.

Table 1
Shear band spacing at different strain rates

Strain rate (1/s)	Shear band spacing (mm)	
	with geometric softening	without geometric softening
10^3	1.33	3.720
10^4	0.233	0.625
10^5	0.0398	0.100

hardening exponent m. However, for a larger range of values of $n/0.107$ between 0 and 5, L_s first increases with n till $n/0.107 \simeq 2.5$ and then decreases; e.g., see Fig. 6g.

Fig. 6h,i exhibits the dependence of the SBS on the thermal softening exponent ν for various values of the strain and the strain-rate hardening exponents n and m. There is no scaling law between L_s and ν. For ν close to 5.0 the SBS seems to be independent of the strain hardening exponent n. However, we can conclude from the plot of Fig. 6i that for $10^{-6} \leqslant m \leqslant 2 \times 10^{-2}$ the SBS is essentially independent of ν.

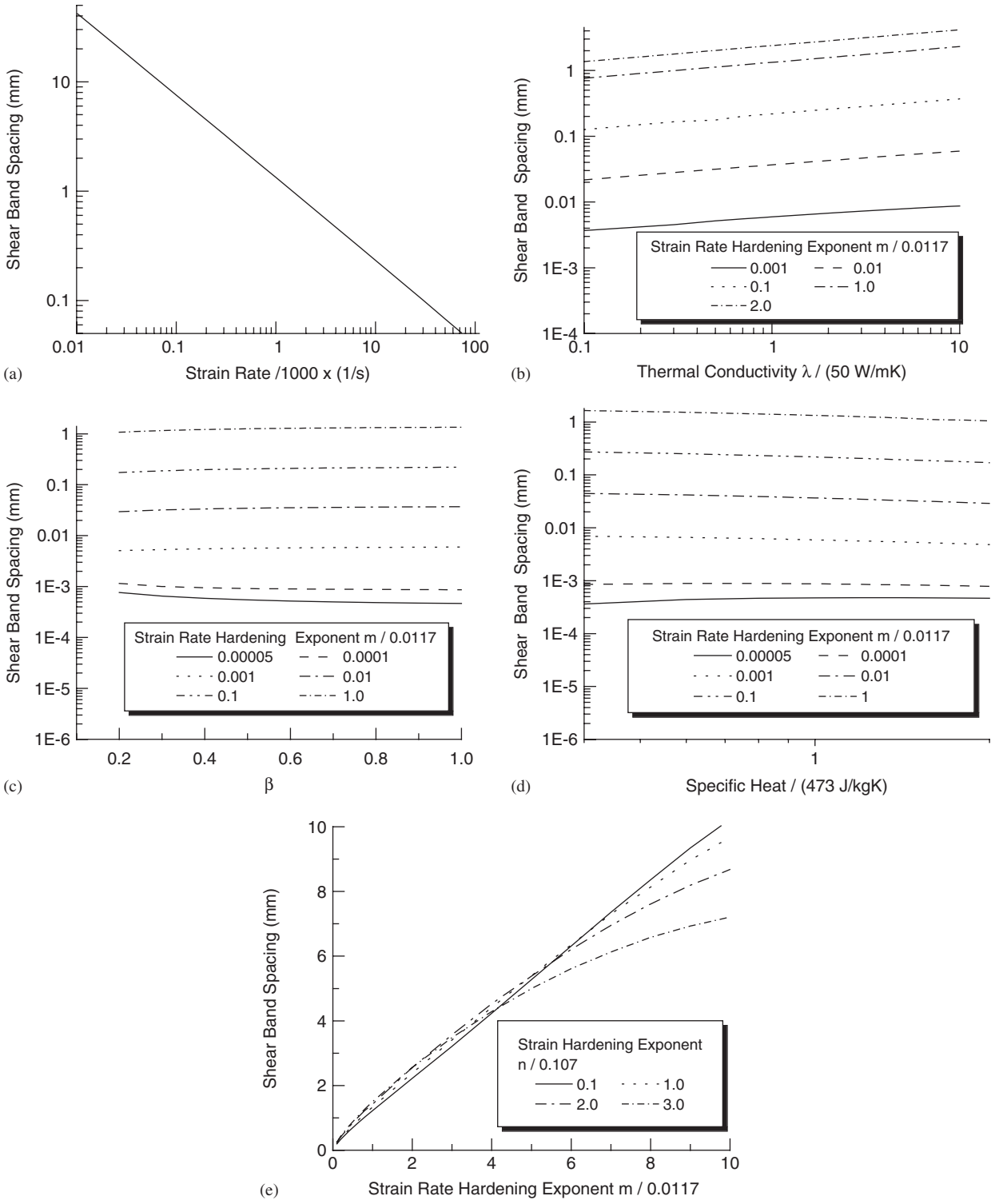

Fig. 6. Dependence of the shear band spacing upon (a) the axial strain rate, (b) the thermal conductivity, (c) the Taylor–Quinney parameter, (d) the specific heat c, (e) the strain-rate hardening exponent m, (f,g) the strain hardening exponent and (h,i) the thermal softening exponent v.

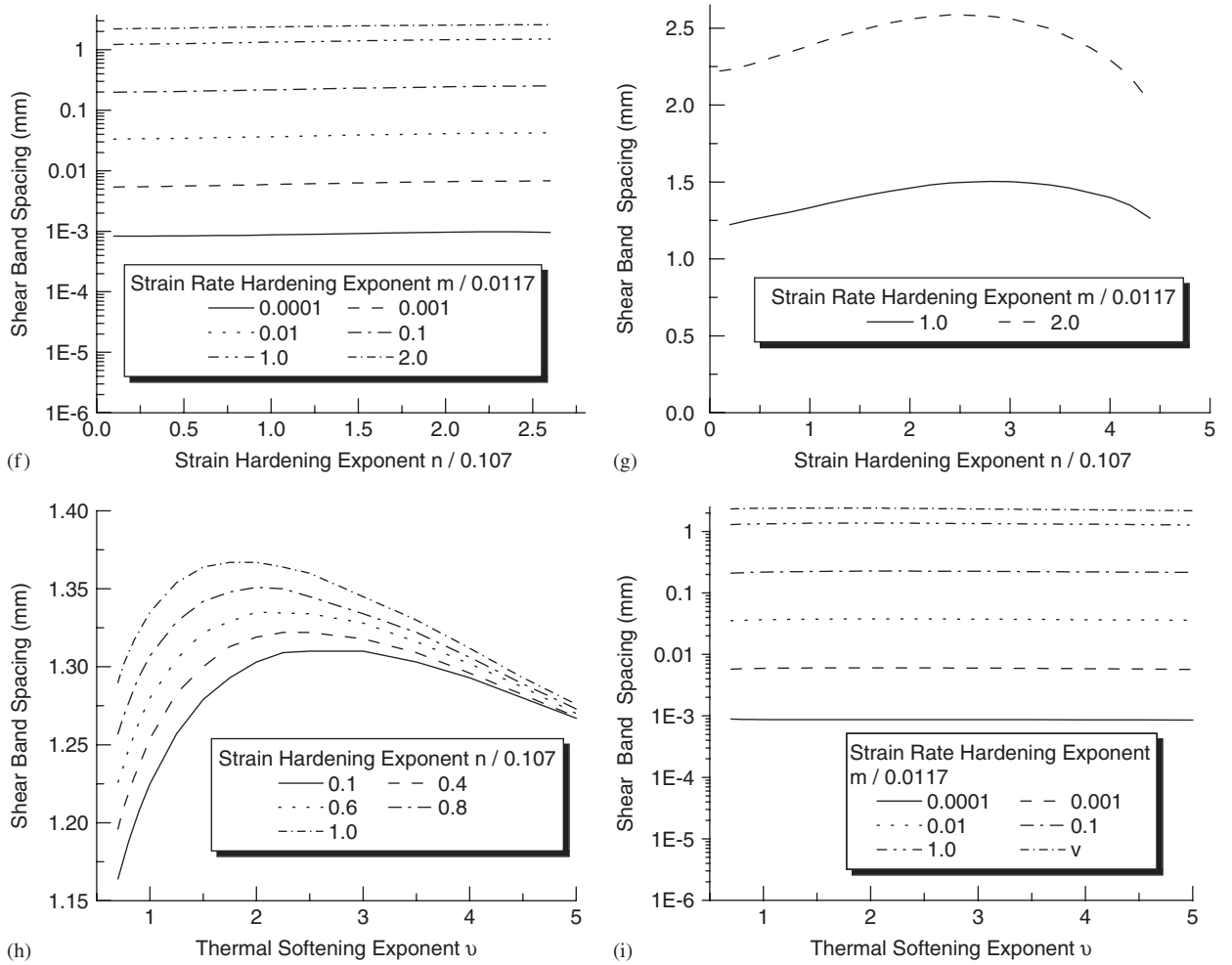

Fig. 6. (*Continued*)

In summary, $L_s \propto (\dot{\varepsilon}_0)^{-0.757}$ and $L_s \propto \lambda^{\bar{\chi}}$ where $\bar{\chi}$ varies with the value of the strain hardening exponent m. Except for the dependence of the SBS upon the nominal axial strain rate, the dependence of L_s upon other material parameters for simple tensile deformations is quite different from that for simple shearing deformations.

7.2.3. Comparison with experimental data

There is no experimental data available on SBS in simple tension. However, recalling that the effective plastic strain rate in a shear band is $\sim 10^5$/s, values of SBS found herein are of the same order of magnitude as those determined experimentally by Xue et al. [10] in explosively loaded cylinders.

7.2.4. Remarks

It is interesting to note that the exponent of the dependence of the SBS on the nominal strain rate is ~ -0.75 both for simple shear and simple tensile deformations. It thus appears that the exponent is an intrinsic characteristic of the SBS, and is essentially independent of the state of stress.

For the problem studied herein there are two characteristic length scales: one due to heat conduction/diffusion, and other due to viscosity or momentum diffusion. The former equals $(t\lambda/\rho c)^{1/2}$ and the latter

$((1/\rho\dot{\varepsilon})(\partial\sigma/\partial\dot{\varepsilon}))^{1/2}$. For the constitutive relation (30), the thermal length varies as $\dot{\varepsilon}_0^m$ and the viscous length as $m\dot{\varepsilon}_0^{(m/2)-1}$. It thus appears that the viscous length determines the SBS.

Numerical experiments of Batra [27], Batra and Kim [28], and Kwon and Batra [29] tend to support the SBS postulate (26) for simple materials but not for strain-rate gradient-dependent materials. They perturbed the homogeneous solution by introducing a finite size temperature perturbation with multiple cusps and numerically solved the resulting nonlinear problem. Kwon and Batra [29] found that, for simple materials an ASB formed at each trough in the cosine wave in the specimen deformed at an average strain-rate $\dot{\varepsilon}_0$ of 500/s but at each crest for $\dot{\varepsilon}_0 = 50\,000$/s. For strain-rate gradient-dependent materials, an ASB formed at each of the two bounding surfaces for $\dot{\varepsilon}_0 = 500$/s, and multiple ASBs formed at each crest when $\dot{\varepsilon}_0 = 50\,000$/s. These authors considered finite perturbations that satisfied boundary conditions, and did not investigate the dependence of the SBS upon the finite element mesh used. As noted by Batra [27] there are several length scales in strain-rate gradient-dependent materials; their effect on the SBS has not been delineated.

Batra and Liu [30] have analyzed the initiation and development of ASBs in plane strain compression of a thermoviscoplastic body of square cross-section. They assumed deformations to be symmetric about the horizontal and the vertical centroidal axes and introduced two perturbations at points located on the vertical centroidal axis that were equidistant on either side of the horizontal centroidal axes. It is hard to find the SBS from the computed shear band pattern.

Batra and Love [31] have recently analyzed the initiation and development of ASBs in a particulate composite comprised of tungsten particulates in a NiFe matrix. Thermophysical parameters of each material were considered in the analysis. Thus, there are numerous sources to make the deformation inhomogeneous. Even though more than one ASB formed in plane strain tension/compression and axisymmetric tensile deformations, the SBS could not be computed.

We note that the SBS based on perturbation analysis equals characteristic distance between nuclei of ASBs, and not the distance between well-developed ASBs; the difference in self-organization of these two different objects is discussed in [10]. The perturbation analysis gives a lower bound for the SBS.

The present work illustrates the effect of geometric softening/hardening on the SBS, and is useful for analyzing the effects of combined shear and tensile/compressive loading, as well as for studying the effect of softening induced due to damage.

8. Conclusions

We have delineated the effect of geometric softening/hardening on the instability strain and the shear band spacing in axial tensile/compressive deformations of a bar made of an isotropic heat-conducting thermoviscoplastic material. It is found that geometric softening significantly affects the instability strain and the shear band spacing; both decrease noticeably when the reduction in the area of cross-section is considered. The instability strain is affected very little by the damage evolution since the instability strain is only ~8% and the damage evolved at the instant of instability is negligible. Out of various material parameters only thermal softening and strain hardening exponents have a noticeable effect on the instability strain. Increasing the strain-rate hardening exponent from 5×10^{-5} to 1 increases the shear band spacing from $\sim 10^{-3}$ to ~1 mm. Enhancing the thermal conductivity from 5 to 500 W/mK raises the shear band spacing from ~0.76 to ~2.3 mm. Both for simple shear and simple tensile deformations the shear band spacing is proportional to the (nominal strain rate)$^{-0.757}$; thus, the exponent -0.757 is independent of the overall stress state. However, other aspects of the scaling law found for simple shearing and simple tensile deformations are quite different. It implies that results obtained for simple shearing deformations cannot be simply carried over to simple tensile/compressive deformations.

Acknowledgements

This work was partially supported by the NSF grant CMS0002849, the ONR grants N00014-98-1-0300 and N00014-03-MP-2-0131, the ARO grant DAAD19-01-1-0657 and the AFOSR MURI to Georgia Institute of Technology with a subcontract to Virginia Polytechnic Institute and State University. Z. G. Wei's work was

also partially supported by the Chinese NSF grant 10002017. Views expressed in the paper are those of authors and not of funding agencies.

References

[1] Considerè M. L'emploi du fer et Lacier Dans Les Constructions. Ann Des Ponts et Chausses 1885;9:574.
[2] Hart EW. Theory of the tensile test. Acta Metall 1967;15:351–5.
[3] Jonas JJ, Baudelet B. Effect of crack and cavity generation on tensile stability. Acta Metall 1977;25:43–50.
[4] Kocks UF, Jonas JJ, Mecking H. The development of strain-rate gradients. Acta Metall 1979;27:419–32.
[5] Ferron G. Influence of heat generation and conduction on plastic stability under uniaxial tension. Mater Sci Eng 1981;49:241–8.
[6] Fressengeas C, Molinari A. Inertia and thermal effects on the localization of plastic flow. Acta Metall 1985;33:387–96.
[7] Shockey DA, Erlich DC. Metallurgical influences on shear band activity. In: Meyers MA, Murr LE, editors. Shock wave and high-strain-rate phenomena in materials. 1981. p. 249–61.
[8] Shockey DA. Materials aspects of the adiabatic shear phenomenon. In: Murr LE, Staudhammer KP, Meyers MA, editors. Metallurgical application of shock-wave and high-strain-rate phenomena. 1986. p. 633–56.
[9] Nesterenko VF, Meyers MA, Wright TW. Self-organization in the initiation of adiabatic shear bands. Acta Mater 1995;46:327–40.
[10] Xue Q, Meyers MA, Nesterenko VF. Self-organization of shear bands in titanium and Ti-6Al-4V alloy. Acta Mater 2002;50:575–96.
[11] Grady DE, Kipp ME. The growth of unstable thermoplastic shear with application to steady-wave shock compression in solids. J Mech Phys Solids 1987;35:95–118.
[12] Grady DE. Properties of an adiabatic shear band process zone. J Mech Phys Solids 1992;40:1197–215.
[13] Bai YL, Cheng CM, Ling Z. Localization and pattern of deformation in thermo-visco-plastic material. J Mech Behav Mater 1992;4:19–32.
[14] Bai YL. Thermo-plastic instability in simple shear. J Mech Phys Solids 1982;30:195–207.
[15] Wright TW, Ockendon H. A scaling law for the effect of inertia on the formation of adiabatic shear bands. Int J Plasticity 1996;12:927–34.
[16] Molinari A. Collective behavior and spacing of adiabatic shear bands. J Mech Phys Solids 1997;45:1551–75.
[17] Batra RC, Chen L. Shear band spacing in gradient-dependent thermoviscoplastic materials. Comput Mech 1999;23:8–19.
[18] Batra RC, Chen L. Effect of viscoplastic relations on the instability strain, shear band initiation strain, the strain corresponding to the minimum shear band spacing, and the band width in a thermoviscoplastic material. Int J Plasticity 2001;17:1465–89.
[19] Chen L, Batra RC. Microstructural effects on shear instability and shear band spacing. Theor Appl Fracture Mech 2000;34:155–66.
[20] Batra RC, Chen L. Instability analysis and shear band spacing in gradient-dependent thermoviscoplastic materials with finite speeds of thermal waves. Arch Mech 2001;53:167–92.
[21] Batra RC, Wei Z. Shear band spacing in thermoviscoplastic materials. Int J Impact Eng 2006;32:947–67.
[22] Rice JR, Tracey DM. On the ductile enlargement of voids in triaxial stress fields. J Mech Phys Solids 1969;17:210–7.
[23] Bai YL, Ke FJ, Xia MF. Formulation of statistical evolution of microcracks in solids. Acta Mech Sinica 1991;7:59–66.
[24] Bai YL, Bai J, Li HL, Ke FJ, Xia MF. Damage evolution localization and failure of solids subjected to impact loading. Int J Impact Eng 2000;24:685–701.
[25] Wei ZG, Batra RC. Dependence of instability strain upon damage in thermoviscoplastic materials. Arch Mech 2002;54:691–707.
[26] Batra RC, Lear MH. Adiabatic shear banding in plane strain tensile deformations of 11 thermoviscoplastic materials with finite thermal wave speed. Int J Plasticity 2005;21:1521–45.
[27] Batra RC. The initiation and growth of, and the interaction among adiabatic shear bands in simple and dipolar materials. Int J Plasticity 1987;3:75–89.
[28] Batra RC, Kim CH. The interaction among adiabatic shear bands in simple and dipolar materials. Int J Eng Sci 1990;28:927–42.
[29] Kwon YW, Batra RC. Effect of multiple initial imperfections on the initiation and growth of adiabatic shear bands in nonpolar and dipolar materials. Int J Eng Sci 1988;26:1177–87.
[30] Batra RC, Liu D-S. Adiabatic shear band development in dynamic plane strain compression of a viscoplastic material. Int J Plasticity 1990;6:231–46.
[31] Batra RC, Love BM. Mesoscale analysis of shear bands in high strain rate deformations of tungsten/nickel-iron composites. J Therm Stresses 2005;28:747–82.